Results in Physics 8 (2018) 438–441

Contents lists available at ScienceDirect

Results in Physics

journal homepage: www.journals.elsevier.com/results-in-physics

# A novel plasmonic interferometry and the potential applications

J. Ali [a], N. Pornsuwancharoen [b], P. Youplao [b], M.S. Aziz [a], S. Chiangga [c], J. Jaglan [d,e], I.S. Amiri [d,f], P. Yupapin [d,e,*]

[a] Laser Centre, IBNU SINA ISIR, Universiti Teknologi Malaysia, 81310 Johor Bahru, Malaysia
[b] Department of Electrical Engineering, Faculty of Industry and Technology, Rajamangala University of Technology Isan, Sakon Nakhon Campus, 199 Phungkon, Sakon Nakhon 47160, Thailand
[c] Department of Physics, Faculty of Science, Kasetsart University, Bangkok 10900, Thailand
[d] Computational Optics Research Group, Advanced Institute of Materials Science, Ton Duc Thang University, District 7, Ho Chi Minh City, 700000, Viet Nam
[e] Faculty of Electrical & Electronics Engineering, Ton Duc Thang University, District 7, Ho Chi Minh City, 700000, Viet Nam
[f] Division of Materials Science and Engineering, Boston University, Boston, MA, 02215, USA

ARTICLE INFO

*Article history:*
Received 7 October 2017
Received in revised form 7 December 2017
Accepted 18 December 2017
Available online 22 December 2017

ABSTRACT

In this article, we have proposed the plasmonic interferometry concept and analytical details given. By using the conventional optical interferometry, which can be simply calculated by using the relationship between the electric field and electron mobility, the interference mobility visibility (fringe visibility) can be observed. The surface plasmons in the sensing arm of the Michelson interferometer is constructed by the stacked layers of the silicon-graphene-gold, allows to characterize the spatial resolution of light beams in terms of the electron mobility down to 100-nm scales, with measured coherence lengths as low as ~100 nm for an incident wavelength of 1550 nm. We have demonstrated a compact plasmonic interferometer that can apply to the electron mean free paths measurement, from which the precise determination can be used for the high-resolution mean free path measurement and sensing applications. This system provides the practical simulation device parameters that can be fabricated and tested by the experimental platform.


## Introduction

Conventional interferometer is recognized as a very important instrument for long range or relative distance measurement many years ago [1], while application in the optical fiber optic sensors was also well established and interesting [2]. Recently Pornsuwancharoen et al. have shown the very promising device based on the plasmonic aspect, in which the system consists of the stacked layers of silicon-graphene-gold that can be integrated as the plasmonic device [3], while the use of the plasmonic behaviors to form the interferometer was also reported and found interesting [4–7]. Experiments have been done in an effort to demonstrate such behaviour that is established with Michelson interferometer as an optical constant. However, the use of such behaviors for a Michelson interferometer has not been addressed well established. By using the ring resonator in the form of the add-drop filter, the classical Michelson interferometer can be formed [8].

From the given relationship $V_d = \mu E$, where the magnitude of the electron drift velocity is $V_d$ caused by the electric field, E is the magnitude of the electric field applied to a material, and $\mu$ is the electron mobility of material. In this case, the electron drift velocity in the studied material (gold) is modulated by the plasmon waves from silicon to graphene as shown in Fig. 1. The driven electron driven mobility is obtained by the driven group velocity injected by the silicon-graphene plasmonic waves [9], which provides the increase in electron mobility. *Since* $I \propto E^2$, therefore the irradiance output at the detector as the function of the recovery arm (optical path difference, $\Delta l$) of the Michelson interferometer, can be seen in the form of the interference fringe (mobility visibility) by scanning the recovery sensing arm, which is the reference arm. The relationship of the interference fringe in terms of the mobility visibility of the plasmonic interferometer can be written by [8]

$$I(\Delta l) = I_0\left(k_{12}^2 k_{22}^2 r_A^2 + k_{13}^2 k_{32}^2 r_B^2\right)\left[1 + V(\Delta l)cos\left(2\frac{2\pi}{\lambda_0}N[D - \Delta l(1 - p_e)]\right)\right] \quad (1)$$

where $\boldsymbol{I}$ is the output irradiance (Mobility), V is the contrast of the interferometer, D is the arm length difference (Optical path difference, OPD), $\boldsymbol{I}_0$ is the input source irradiance (Mobility), N is the effective refractive index of the waveguide, $\lambda_0$ is the light source wavelength, $p_e = 0.22$ is the elastic coefficient of the waveguide,

* Corresponding author at: Computational Optics Research Group, Advanced Institute of Materials Science, Ton Duc Thang University, District 7, Ho Chi Minh City, 700000, Viet Nam.
*E-mail address:* preecha.yupapin@tdt.edu.vn (P. Yupapin).

https://doi.org/10.1016/j.rinp.2017.12.055
2211-3797/

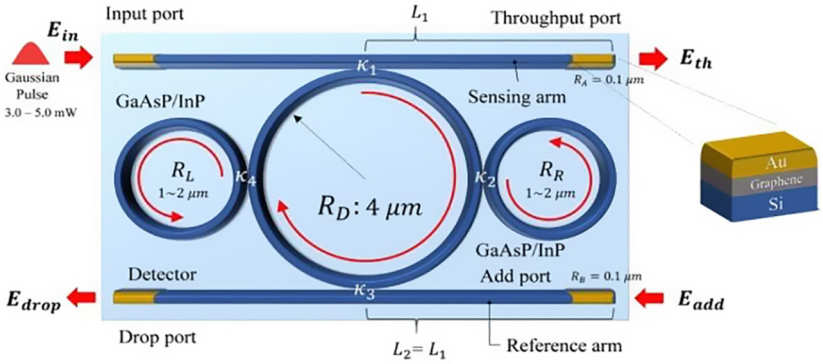


**Fig. 1.** A schematic plasmonic interferometer, where $R_D, R_R, R_L$, are the ring radii of the center ring and two side rings, right $(R_R)$ and left $(R_L)$ hands. The sensing and reference arms, input and drop ports are connected by the stacked silicon-graphene-gold layers, $K_1 = K_2 = K_3 = K_4 = 0.5$, the waveguide loss is 0.1 dB mm$^{-1}$.

$k_{ij}$ are the coupling coefficients, $r_A, r_B$: Reflection coefficients of the waveguide ends.

We assume that the change in the gold layer length is not larger than the elongation limit, yields [8]

$$V(\Delta l) = \frac{k_{12}k_{22}r_A k_{13}k_{32}r_B}{k_{12}^2 k_{22}^2 r_A^2 k_{13}^2 k_{32}^2 r_B^2}\left(\sum_{q=1}^{p} H_q\right)^{-1} \cdot exp\left[-\left(\frac{\pi N}{\sqrt{\ln 2}}\frac{\Delta\lambda}{\lambda_0^2}[D-\Delta l(1-p_e)]\right)^2\right] \times \sqrt{\left(\sum_{q=1}^{p} H_q \cos(A)\right)^2 + \left(\sum_{q=1}^{p} H_q sin(A)\right)^2} \quad (2)$$

where $A = \left(\mathbf{2}\frac{2\pi}{\lambda_0^2}\Delta\lambda_1(\boldsymbol{q}-1)\boldsymbol{N}[\boldsymbol{D}-\Delta\boldsymbol{l}(1-\boldsymbol{p_e})]\right)$, $\lambda_0$ is the input source wavelength, $\Delta\lambda$ is the spectral width, $\Delta\lambda_1$ is the mode spacing, $H_q$ is the amplitude of the q$^{th}$ of the output mobility mode and $D$ is the initial interferometer arm length difference.

In Fig. 1, the electron mobility in gold on the sensing arm can be changed by the change in a gold layer length by the external physical parameters such as current, voltage, heat etc., which can be recovered by scanning the reference arm and seen on the mobility visibility when the balanced mobility visibility is obtained. From which the scanning range in terms of the mobility path difference $(\Delta l)$ is measured, which is related to the electron mobility or mean free paths. Principally, the electrical mobility(μ) is a value directly related to electrical conductivity which is given by $\boldsymbol{\mu} = \frac{e\tau}{m} = \frac{ed}{mv_F}$ [10], where e is the charge, τ is the mean free time, m is the mass, d is the mean free paths, and $v_F$ is the Fermi velocity of the charge carrier. The Fermi velocity can easily be derived from the Fermi energy via the non-relativistic kinetic energy equation. However, the gold film thickness can be smaller than the predicted mean free paths, making surface scattering much more noticeable, effectively increasing the resistivity. The values of the electron mean free path are also found in the reference [11].

The plasmonic in the following details in which the conventional interferometry mechanism is described as the Michelson interferometer requires the two equal lengths of the interferometric arms at the initial state, which is the balanced position. These two arms are the "sensing" and "reference" arms. From Fig. 1, all device ports are made of the short length of the stacked silicon-graphene-gold layers. In the measurement, the change caused by the external physical parameters such as heat, bias current (voltage), pressure are coupled into the graphene and silicon layers, which affect to the balanced interferometer position. From which the measurement recovery of the change can be applied and the measured values obtained when the interferometer is at the balanced position, where the interference signals are observed by detection by the photo-detector (photon counter) at the drop port output. In the simulation, the input light is input into the input port. Generally, the different detectors such as the photo-detector, photon counter and magnetic sensor can be used for the various aspects of measurements. Firstly, the interference signals in the form of the output intensity visibility can be detected by the photo-detector, in which the interference occurs within the silicon layer will be seen by the scanning the recovery OPD, which is the conventional interferometer. Secondly, the mobility visibility caused by the change of the excited electron in the gold layer is observed by the by the same method but the mobility visibility is seen by the change of the output light group velocity [9]. Thirdly, the photon distribution within the interferometer which is the quantum picture can also be detected by the photon counter, where the entangled photon can be measured and configured. Furthermore, the gold material layer can be substituted by the ferromagnetic material, where in this case the detected outputs are the electron spins up and down energy distributions, which can be observed by the magnetic sensor. This type of the device is called the spintronic interferometer, where the measurement resolution can be increased by the very short spin time of the electron [9].

In a simulation, light from a laser is input into the input port as shown in Fig. 1, where the input peak power is at 0.5 mW, with the wavelength center is at 1550 nm. The light is entered into the interferometer, where the fraction of light is coupled to the center ring and a right side ring, the other part of light propagates to the sensing arm (Through port). The fraction of light then reflected into the system and the input port and the center ring and side ring via the same coupler. From which the combination of light signals with different phases is coupled into the center ring and coupled to the drop port via the second coupler, then the light is coupled into the left side ring and center ring, respectively, which is shown in Fig. 2. Then the light is coupled into the first coupling point and following the same pattern until the resonance occurs. The measurement output at the drop port is obtained by using an Eq. (1), where finally the output intensity can be changed to the electron group velocity and mobility by the given relationship. The change in electron mobility and the recovery at the sensing arm and the reference (scanning range) can be seen at the drop port output when the balanced mobility visibility is achieved. In practice, the mobility visibility contrast can be controlled and adjusted by controlling the parameters the Eq. (2). In Fig. 3, the relationship between the change in the electron mobility and the gold layer length of the sensing arm is plotted, in which the linear relationship is seen when the gold length is less than 100 nm. In Fig. 4, the plot of the relationship between the input power and the change in electron mobility as the sensing arm (Through port) of the system is characterized by the relationship $\mathbf{I} = E^2 = \left(\frac{V_d}{\mu}\right)^2$, $V_d$

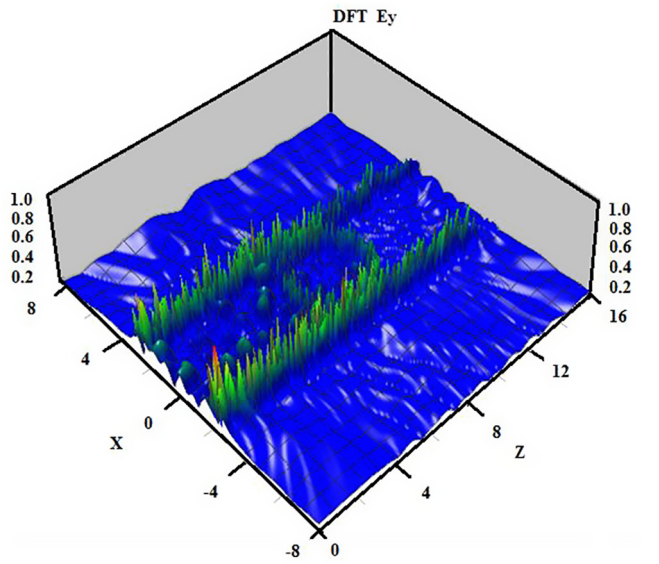


**Fig. 2.** Shows the 3D Opti-wave result of the system in Fig. 1 for preliminary investigation, the parameters are $R_L = 1.4\ \mu m$, $R_R = 1.5\ \mu m$ and $R_D = 2.0\ \mu m$. The sensing and reference arm reflectivity is 0.04 (4%).

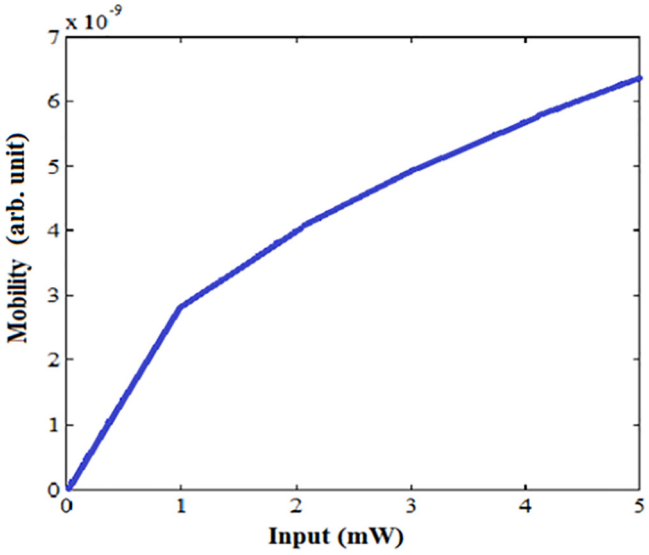


**Fig. 3.** Plot of the gold layer mobility and the change in gold layer length ($\Delta l$), with the $\Delta l$ resolution = 100 nm, the input power is fixed at 0.5 mW, where the maximum ($\Delta l$) is 600 nm. The linear relationship is observed at ($\Delta l$) = 100 nm.

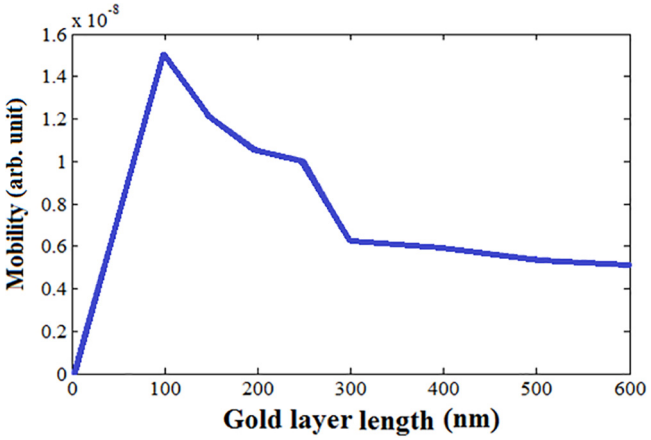


**Fig. 4.** Plot of the gold layer mobility and the input power, the maximum power is 5.0 mW, where the change in gold layer length ($\Delta l$) of the sensing arm is fixed at 100 nm.

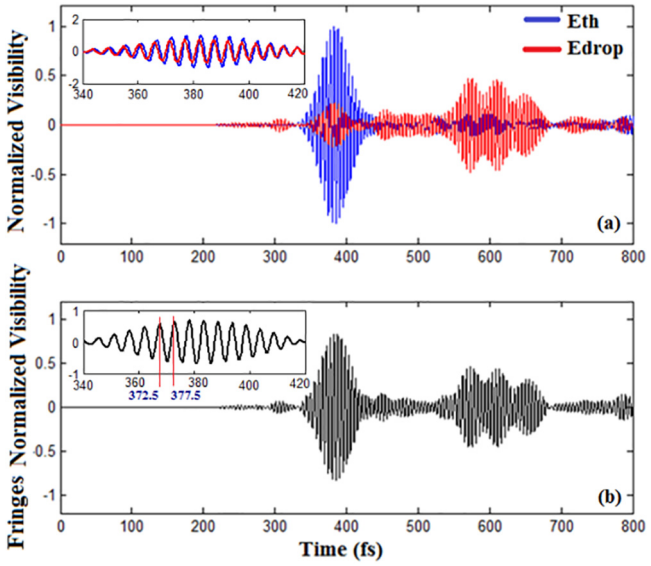


**Fig. 5.** Plot ($\Delta l$) and the change in mean free paths, $\boldsymbol{\mu = \frac{e\tau}{m} = \frac{ed}{mv_F}}$, **where** $\boldsymbol{V_F = 10^5\ ms^{-1}}$ of electron in gold [10], the electron mobility in gold is 42.6 $cm^2\ V^{-1}\ s^{-1}$, the input power is fixed at 0.5 mW, the electron mass is $9.10 \times 10^{-31}$ kg, the electron charge is $1.60 \times 10^{-19}$ C. The refractive indices of a silicon and GaAsInP/P are 1.46 and 3.14, respectively. The fringe peak to peak is obtained at $\Delta t$ = 5 fs, is $1.0 \times 10^{-7}$m or 100 nm, where (a) the blue color is the through port output signals and the red color is the drop port output signals, (b) the black and white signals of (a). The interference fringes of the interferometer are seen at the drop port. In this case $\Delta l$ is also additionally obtained from the right and left two side rings in terms of the phase differences. (For interpretation of the references to color in this figure legend, the reader is referred to the web version of this article.)

is the group velocity, where the linear relationship of the power and mobility is seen. The output mobility visibility is plotted in Fig. 5, which is shown the mobility visibility, when ($\Delta l$) is fixed at 0.0 μm. The plot is obtained by the relationship between the electron mobility in the gold layer and the light intensity, which is the same as the light intensity in an Eq. (1). The coupling constants of the coupler are given in Fig. 1. The obtained fringe peak to peak resolution is 100 nm. However, the resolution can be improved by the two side ring (phase modulator) parameters in terms of ring radii and materials.

In conclusion, we have realized that the applied physical parameters such as bias current (voltage), heat, force pressure etc. can apply to the sensing arm, from which the electron with the gold layer can be directly/indirectly excited and changed the overall electron mobility, which is affected the change in mobility visibility, while the superposition of the electrons can be averaged and the mean free path calculated, which is also useful for the mean free path measurement and sensing applications. In physics, the mean free path is the average distance travelled by a moving particle (such as an atom, a molecule, a photon) between successive impacts (collisions), which its direction or energy or other particle properties is modified. This concept can be applied to any conducted materials, where the changes in the mean free path can be measured by the proposed interferometer. In which the mobility fringe is formed by the mobility visibility of the plasmonic interferometer. The measurement resolution can also be improved by the adjusting the two side ring parameters, which is the phase modulators made of the nonlinear material, is a **GaAsInP/P,** from

which the nonlinear effect is coupled into the center ring and required fringe width can be desired and obtained, which is useful for the optical path difference i.e. mean free path improvement.

## Acknowledgments

The authors would like to give the appreciation for the research financial support and the research facilities from the Universiti Teknologi Malaysia, Johor Bahru, Malaysia.

## Appendix A. Supplementary data

Supplementary data associated with this article can be found, in the online version, at https://doi.org/10.1016/j.rinp.2017.12.055.

## References

[1] Shoemaker D, Fritschel P, Giaime J, Christensen N, Weiss R. Prototype michelson interferometer with fabry-perot cavities. Appl Opt 1991;30 (22):3133–8.
[2] Weir K, Boyle WJO, Meggit BT, Palmer AW, Grattan KTV. A novel adaptation of the Michelson interferometer for the measurement of vibration. Lightwave Technol 1992;10(5):700–3.
[3] Pornsuwancharoen P, Amiri IS, Suhailin FH, Aziz MS, Ali J, Singh G, Yupapin P. Micro-current source generated by a WGM of light within a stacked silicon-graphene-Au waveguide. IEEE Photon Technol Lett 2017;29(21):1768–71.
[4] Graydon O. Plasmonic interferometry. Nat Photon 2012;6(3):139.
[5] Feng JV, Siu S, Roelke A, Mehta V, Rhieu SY, Tayhas G, Palmore R, Pacifici D. Nanoscale plasmonic interferometers for multispectral, high-throughput biochemical sensing. Nano Lett 2011;12(2):602–9.
[6] Morrill D, Li D, Pacifici D. Measuring subwavelength spatial coherence with plasmonic interferometry. Nat Photon. 2010;10:661–87.
[7] Li D, Feng J, Pacifici D. Nanoscale optical interferometry with incoherent light. Sci. Rep 2016. Article number 20836.
[8] Szuatakowski M, Palka N. Contrast sensitive fiber optic Michelson interferometer as elongation sensor. Opto-electron. Rev. 2005;13(1):19–26.
[9] Pornsuwancharoen N, Youplao P, Amiri IS, Ali J, Yupapin P. Electron driven mobility model by light on the stacked metal-dielectric-interfaces. Microw Opt Tech Lett 2017;59(7):1704–9.
[10] Bourke JD, Chantler CT. Measurements of electron inelastic mean free paths in materials. Phys Rev Lett 2010;104:206601.
[11] Gall D. Electron mean free path in elemental metals. J Appl Phys 2016;119:085101.